Phase and coherence of optical microresonator frequency combs

William Loh,* Pascal Del'Haye, Scott B. Papp, and Scott A. Diddams
National Institute of Standards and Technology, Boulder, Colorado 80305, USA
(Received 11 February 2014; published 9 May 2014)

We use a combination of theoretical analysis, numerical simulation, and experimental measurement to investigate the near-threshold phase and coherence properties of parametric optical frequency combs generated in low-loss dielectric microresonators. Our analysis reveals that near threshold the phases of the comb lines do not stabilize to a constant value across the spectrum, although well-defined phase relationships relative to the pump laser do exist. Our results are supported by numerical simulations of two different microresonator combs operated under varying conditions of input drive, dispersion, and detuning. These results are also experimentally confirmed through phase measurements of the individual comb lines. We also investigate the processes leading to the breakdown of the equidistant frequency spacing of the modes in a microresonator comb.

DOI: 10.1103/PhysRevA.89.053810 PACS number(s): 42.62.Eh, 42.65.Ky, 42.65.Re, 42.65.Yj

I. INTRODUCTION

An optical frequency comb [1–3] consists of an array of equidistant lines in frequency space with a well-defined phase relation between each of the individual comb lines. This phase relation can lead to the buildup of an optical pulse if some of the comb lines constructively interfere at a single instant of time. The optical frequency comb serves as the essential enabler for a variety of applications in spectroscopy, metrology [4], astronomy [5], sensing, and microwave signal generation [6]. Although traditionally produced in the output of a mode-locked laser, frequency combs have recently been generated in microresonators due to the interplay of third-order nonlinear optical processes [7–11].

Solitons [12] and ultrashort pulses [13] have been demonstrated experimentally and predicted theoretically [14–17] as a possible output of the microresonator comb. However, in Ref. [18] it was determined experimentally that the phases of the comb lines generated via four-wave mixing in a microresonator could be stationary in time but not follow any natural order and in many cases can be seemingly random. Within this context, the goal of this work is to investigate the phase relation between the comb lines using a combination of theory, numerical simulation, and experiment. The comb phase is important as it determines the properties of the generated optical pulse train. The optical pulses are shortest when all the phases are aligned, but when the phases are stationary and random, the output is incoherently modulated or even quasicontinuous. Our studies specifically focus on the comb's operation slightly above threshold, treating the case of the pump mode and the first two comb lines generated via degenerate four-wave mixing. We find the comb phases in this case to be stationary but spectrally disordered under ordinary operating conditions. This is significant since the generation of the subsequent comb lines is dependent on these initial comb modes and could therefore lead to a disordered phase arrangement across the full comb. As a separate point of study, we also explore the processes leading to nonequidistance between the generated comb lines. Our results here show the potential for violating equidistance when the secondary comb lines begin to form, as is often reported in experimental measurement [19,20].

II. MICRORESONATOR COMB PHASE ANALYSIS

For our analysis, we consider the simplified configuration of a microresonator comb shown in Fig. 1(a). The analysis of this system follows traditional treatments of optical fields coupled by the four-wave-mixing nonlinearity [21] but modified to account for a microresonator oscillator having nonzero pump detuning [22]. We begin with the coupled-mode equations governing the evolution of the first three comb modes under the excitation of the pump [22–24]

$$\frac{dA_0}{dt} = -\frac{1}{2}\Delta\omega A_0 - ig_0|A_0|^2 A_0 - 2ig_0 A_l A_{-l} A_0^* e^{-i\varpi_l t} + \frac{1}{2}\Delta\omega F_0 e^{i\sigma t}, \quad (1)$$

$$\frac{dA_{\pm l}}{dt} = -\frac{1}{2}\Delta\omega A_{\pm l} - 2ig_0|A_0|^2 A_{\pm l} - ig_0 A_0^2 A_{\mp l}^* e^{i\varpi_l t}.$$

Here A_0 represents the normalized complex field of the mode excited by the pump, while $A_{\pm l}$ denotes the mode pair on the higher (+) and lower (–) frequency side l cavity resonances away from A_0. In Eq. (1), $\Delta\omega$ denotes the linewidth of the resonator modes, $|F_0|^2$ denotes the external drive of the pump, and $g_0 = n_2 c\hbar\omega_0^2/n_0^2 V_0$ denotes the gain parameter of the Kerr nonlinearity. Here n_2 is the Kerr nonlinear refractive index of the medium, ω_0 is the angular frequency of the fundamental resonance, n_0 is the real refractive index of the medium, and V_0 is the effective mode volume. The quantity $\varpi_l = 2\omega_0 - \omega_l - \omega_{-l}$ represents the frequency mismatch due to dispersion between the fundamental resonance ω_0 and the frequency of the $\pm l$ resonances $\omega_{\pm l}$. Here $\sigma = \Omega_0 - \omega_0$ represents the detuning of the pump frequency Ω_0 from the fundamental cavity resonance. We consider the comb at the onset of oscillation threshold with the Kerr interactions existing primarily between three resonator modes. In Eq. (1) we assume that the losses are approximately equal for the three modes considered, that the intermodal coupling containing the spatial overlap [22] is nearly unity for these three modes, and that $|A_0|$ is significantly stronger than $|A_{\pm l}|$ so that the nonlinear phase shifts are dominated by $|A_0|^2$.

*william.loh@nist.gov

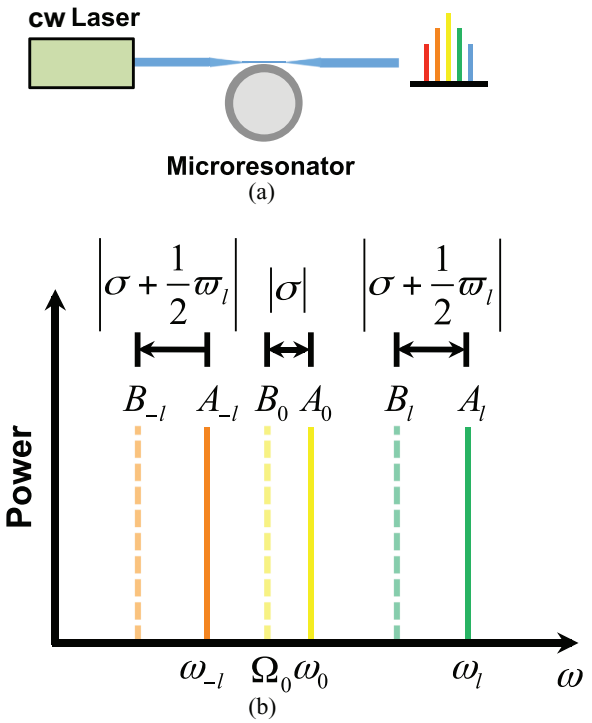

FIG. 1. (Color online) Diagram of (a) the microresonator comb setup and (b) the frequency shift of the comb modes under the transformation from $A_{\pm l}$ to $B_{\pm l}$. The other parameters are defined in the text.

The time dependences of Eq. (1) can be removed if one defines $B_0 = A_0 e^{-i\sigma t}$ and $B_{\pm l} = A_{\pm l} e^{-i(\sigma+\varpi_l/2)t}$ [22], effectively mapping the original cavity modes onto a new set of fields. Under this mapping, Eq. (1) becomes

$$\begin{aligned}\frac{dB_0}{dt} &= -\frac{1}{2}\Delta\omega B_0 - i\sigma B_0 - ig_0|B_0|^2 B_0 \\ &\quad - 2ig_0 B_l B_{-l} B_0^* + \frac{1}{2}\Delta\omega F_0, \\ \frac{dB_{\pm l}}{dt} &= -\frac{1}{2}\Delta\omega B_{\pm l} - i\left(\sigma+\frac{1}{2}\varpi_l\right)B_{\pm l} \\ &\quad - 2ig_0|B_0|^2 B_{\pm l} - ig_0 B_0^2 B_{\mp l}^*.\end{aligned} \tag{2}$$

This transformation can be interpreted using the diagram of the microresonator modes in Fig. 1(b). The complex time-dependent field of the lth comb line can be formulated as $E_l(t) = A_l(t)e^{i\omega_l t}$, which yields $E_l(t) = B_l e^{i(\omega_l+\sigma+\varpi_l/2)t}$ under the previous mapping scheme. For the case of anomalous dispersion (as depicted in Fig. 1), ϖ_l is negative, causing the comb lines at $\pm l$ to each become shifted by a dispersion step towards the lower frequency side. This frequency shift removes the asymmetry in the mode separation. Note that the detuning towards lower frequencies (red detuning $\sigma < 0$) in Fig. 1 provides a constant frequency shift for all the comb lines. Physically, this picture says that the stationary solutions of Eq. (1) are shifted versions of the cavity modes such that equidistance is maintained. This picture of mode translation will become important when we discuss the processes leading to the formation of multiple free-spectral ranges (FSRs) within the microresonator comb.

From Eq. (2) one can proceed along the lines of Ref. [22], perturbing the system from equilibrium and determining the solutions where the perturbations grow over time. These are the solutions where net gain can be achieved with eigenvalues given as

$$\lambda_\pm = \frac{-\Delta\omega \pm \sqrt{-4\sigma_l^2 - 12g_0^2|B_0|^4 - 16\sigma_l g_0|B_0|^2}}{2}, \tag{3}$$

where $\sigma_l = \sigma + \varpi_l/2$. Note that Eq. (3) is derived under the assumptions that the pump depletion is minimal. The mode with the highest gain reaches oscillation first and steady state is achieved when the gain eventually saturates to the level of loss. To determine the combined detuning and dispersion required for the largest gain, we differentiate λ_+ with respect to σ_l, setting the slope to zero. This operation yields

$$\sigma_{l,\mathrm{opt}} = -2g_0|B_0|^2, \tag{4}$$

which agrees with the optimal detuning of Ref. [22] at threshold.

Substituting Eq. (4) into Eq. (2), one finds that the optimal detuning or dispersion occurs when $-i\sigma_l B_{\pm l}$ exactly cancels the cross-phase modulation $-2ig_0|B_0|^2 B_{\pm l}$. This allows for the entirety of the four-wave mixing supplied by the pump ($-ig_0 B_0^2 B_{\mp l}^*$) to be optimally used towards gain. However, as the modes are spaced discretely across the frequency span of the microresonator comb, it is not necessarily true that a pair of modes exist with the exact σ_l for optimum gain. In these cases, the mode pair closest to reaching this condition becomes the oscillating modes of the system.

It can be seen from Eq. (2) that the gain of the four-wave-mixing process is dependent on the phases of the three interacting modes (ϕ_0,$\phi_{\pm l}$). To show this, we first assume that a mode exists where Eq. (4) is exactly satisfied such that the coupled-mode equation for $B_{\pm l}$ simplifies to

$$\frac{dB_{\pm l}}{dt} = -\frac{1}{2}\Delta\omega B_{\pm l} - ig_0 B_0^2 B_{\mp l}^*. \tag{5}$$

Next assuming the phases of $B_0 = |B_0|e^{i\phi_0}$ and $B_{\pm l} = |B_{\pm l}|e^{i\phi_{\pm l}}$ to be stationary with time, we find the corresponding intensity equation for $|B_{\pm l}|^2$ to be

$$\begin{aligned}\frac{d|B_{\pm l}|^2}{dt} &= -\Delta\omega|B_{\pm l}|^2 + 2g_0|B_0|^2\,|B_{+l}|\,|B_{-l}| \\ &\quad \times \sin(2\phi_0 - \phi_{+l} - \phi_{-l}).\end{aligned} \tag{6}$$

From Eq. (6) it is clear that to achieve the largest gain, one requires that the condition

$$2\phi_0 - \phi_{+l} - \phi_{-l} = \pi/2 \tag{7}$$

be satisfied. This is the same phase relation required for maximum gain in a conventional parametric amplifier [25].

Equation (7) shows that a solution where all three modes have identical phase *violates* the condition for maximum gain. Indeed, the gain is zero when the phases are aligned. Since the modes of an oscillator tend to stabilize around the point of maximum gain saturating the gain to the level of loss, one can in principle expect the phases of the most basic three-mode comb to stabilize to the condition of Eq. (7). However, many approximations have gone into this analysis and it is useful at this point to review the effects of some

of these approximations. In setting up the coupled-mode equations of Eq. (2), we assumed the presence of only three interacting modes. Generally, the pump and the first pair of generated modes are the strongest in a microresonator comb, making this approximation fairly reasonable. However, as more modes begin to form, the contributions of these modes begin to accumulate. In Eq. (2) we also only account for the cross-phase-modulation contribution of the pump. When other modes become significant, the total nonlinear phase shift is expected to translate the optimum gain condition to a point where σ_l compensates the total phase shift. In Eq. (3) we assumed that the pump was undepleted. A depleted pump is expected only to lower the four-wave-mixing gain of Eq. (5), leaving the condition of optimal gain relatively unaltered.

Finally, in Eq. (5) we assumed that a cavity mode exists where the condition of Eq. (4) is satisfied. Under typical operating conditions this cannot be achieved and the closest mode instead undergoes oscillation. This creates a residual imaginary term such that Eq. (5) becomes

$$\frac{dB_{\pm l}}{dt} = -\frac{1}{2}\Delta\omega B_{\pm l} - ig_0 B_0^2 B_{\mp l}^* + iKB_{\pm l}, \tag{8}$$

where $K = -\sigma_l - 2g_0|B_0|^2$. Because the condition of steady state requires both the real and imaginary contributions to be compensated, the phases of B_0 and $B_{\pm l}$ must shift so as to prevent phase rotation over time. Depending on the relative magnitudes of $\Delta\omega/2$ and K, the phase can stabilize across a range of values.

Our previous analysis shows that many conditions (such as the presence of other interacting modes or the influence of a residual phase) prevent Eq. (7) from becoming a universal law of the microresonator comb. Nevertheless, from this simple three-mode picture, we see that the basic operation of the comb in most cases will *not* intrinsically stabilize around modes with identical phase. However, we note that in the anomalous dispersion case under the condition of extreme pump red detuning, it is possible for Eq. (4) to become violated when the combined detuning and dispersion overcompensates the cross-phase modulation of the system. Under these conditions, a residual phase shift exists in Eq. (5) causing the comb phase to stabilize into a different optimum configuration.

Because of additional four-wave-mixing contributions, higher-order modes of the comb no longer satisfy Eq. (7). Note that the combined dispersion and detuning of these higher-order modes can also no longer exactly compensate the cross-phase modulation. In principle, one can perform a similar coupled-mode analysis with higher orders of comb modes included so that the phase relation of the higher-order modes may be determined. However, the inclusion of even the next two modes greatly increases the complexity of the problem, making an analytical solution difficult to formulate. Instead, we determine the phase relationships of the higher-order modes through an observation of the symmetry between comb modes. We begin with the coupled-mode equations for modes $\pm 2l$ with only its dominant four-wave-mixing contributions included

$$\begin{aligned}\frac{dA_{\pm 2l}}{dt} = &-\frac{1}{2}\Delta\omega A_{\pm 2l} - 2ig_0|A_0|^2 A_{\pm 2l} - ig_0 A_0^2 A_{\mp 2l}^* e^{i\varpi_{2l}t} \\ &- ig_0 A_{\pm l}^2 A_0^* e^{i(2\omega_{\pm l}-\omega_0-\omega_{\pm 2l})t} - 2ig_0 A_{\pm l} A_0 A_{\mp l}^* \\ &\times e^{i(\omega_{\pm l}+\omega_0-\omega_{\mp l}-\omega_{\pm 2l})t}.\end{aligned} \tag{9}$$

Here $A_{\pm 2l}$ denotes the complex fields of the next higher-order mode pair excited by the pump, $\omega_{\pm 2l}$ denotes their associated frequencies, and $\varpi_{\pm 2l}$ is defined through $\varpi_{\pm 2l} = 2\omega_0 - \omega_{2l} - \omega_{-2l}$.

Our goal now is to map $A_{\pm 2l}$ onto a new set of fields such that the time dependence of Eq. (9) can be effectively removed. The result of this mapping determines the steady-state frequencies associated with the $\pm 2l$ comb lines. With the original mapping scheme for A_0 and $A_{\pm l}$ in place (see Fig. 1) and assuming higher-order dispersion processes (beyond second order) to be negligible, we find that modes $\pm 2l$ are constrained such that $B_{\pm 2l} = A_{\pm 2l} e^{-i[\sigma+(2\omega_0-\omega_{2l}-\omega_{-2l})/2]t}$. Thus, the fields at $\pm 2l$ are again translated by a single dispersion step into equidistance dictated by the positions of the original three comb modes. With this mapping scheme, Eq. (9) transforms into

$$\begin{aligned}\frac{dB_{\pm 2l}}{dt} = &-\frac{1}{2}\Delta\omega B_{\pm 2l} - i\left(\sigma + \frac{1}{2}\varpi_{2l}\right)B_{\pm 2l} - 2ig_0|B_0|^2 B_{\pm 2l} \\ &- ig_0 B_0^2 B_{\mp 2l}^* - ig_0 B_{\pm l}^2 B_0^* - 2ig_0 B_{\pm l} B_0 B_{\mp l}^*.\end{aligned} \tag{10}$$

Equation (10) is similar in form to Eq. (2) for modes $\pm l$ but also includes two additional contributions from four-wave mixing.

Defining $B_0 = |B_0|e^{i\phi_0}$, $B_{\pm l} = |B_{\pm l}|e^{i\phi_{\pm l}}$, and $B_{\pm 2l} = |B_{\pm 2l}|e^{i\phi_{\pm 2l}}$, one can expand Eq. (10) into two separate equations that collectively describe the phase and amplitude evolution of modes $\pm 2l$,

$$\begin{aligned}\frac{d|B_{\pm 2l}|}{dt} = &-\frac{1}{2}\Delta\omega|B_{\pm 2l}| + g_0|B_0|^2|B_{\mp 2l}| \\ &\times \sin(2\phi_0 - \phi_{2l} - \phi_{-2l}) \\ &+ g_0|B_{\pm l}|^2|B_0|\sin(2\phi_{\pm l} - \phi_0 - \phi_{\pm 2l}) \\ &+ 2g_0|B_{\pm l}||B_0||B_{\mp l}|\sin(\phi_{\pm l} + \phi_0 - \phi_{\mp l} - \phi_{\pm 2l}), \\ \frac{d\phi_{\pm 2l}}{dt} = &-\left(\sigma + \frac{1}{2}\varpi_{2l}\right) - 2g_0|B_0|^2 \\ &- g_0\frac{|B_0|^2|B_{\mp 2l}|}{|B_{\pm 2l}|}\cos(2\phi_0 - \phi_{2l} - \phi_{-2l}) \\ &- g_0\frac{|B_{\pm l}|^2|B_0|}{|B_{\pm 2l}|}\cos(2\phi_{\pm l} - \phi_0 - \phi_{\pm 2l}) \\ &- 2g_0\frac{|B_{\pm l}||B_0||B_{\mp l}|}{|B_{\pm 2l}|}\cos(\phi_{\pm l} + \phi_0 - \phi_{\mp l} - \phi_{\pm 2l}).\end{aligned} \tag{11}$$

Note that the dispersion and detuning of Eq. (2), which originally compensated the cross-phase modulation of modes $\pm l$ [see Eq. (4)], now overcompensate the cross-phase modulation of modes $\pm 2l$, yielding a residual phase contribution in Eq. (11).

The *four* evolution equations of Eq. (11) must all independently yield the value of zero at steady state. To proceed further, it becomes necessary to assume that the higher and lower frequency (+ and −) modes of each order are similar in amplitude. This amplitude equality is typical of combs generated in both experimental measurement and numerical simulation, but can also be reasoned to be the configuration that maximizes the gain for each respective mode. In addition, one may also justify this assumption from an argument based

on the symmetry in the coupled-mode equations. Note that it would appear from Eq. (11) that because the phases of the modes are asymmetric, the coupled-mode equations then are asymmetric between the ± modes. At this stage of analysis, careful attention to this point is certainly warranted. Our strategy then is to first begin our analysis assuming equality of amplitudes between the ± modes in each order. By the end, we will show that our solution does not contradict the symmetry of the coupled-mode equations, even with an asymmetry in the comb phase.

Assuming the ± mode amplitudes to be equal, one finds that the first two terms of the amplitude equation and the first three terms of the phase equation are common to modes $\pm 2l$. For all four equations to independently yield zero, the remaining terms of each equation in the $+2l$ mode must balance their counterparts in the $-2l$ mode. We therefore require

$$\begin{aligned}&\sin(2\phi_{+l}-\phi_0-\phi_{+2l})+2\sin(\phi_{+l}+\phi_0-\phi_{-l}-\phi_{+2l})\\&\quad=\sin(2\phi_{-l}-\phi_0-\phi_{-2l})+2\sin(\phi_{-l}+\phi_0-\phi_{+l}-\phi_{-2l})\end{aligned}\tag{12}$$

from the amplitude equations and

$$\begin{aligned}&\cos(2\phi_{+l}-\phi_0-\phi_{+2l})+2\cos(\phi_{+l}+\phi_0-\phi_{-l}-\phi_{+2l})\\&\quad=\cos(2\phi_{-l}-\phi_0-\phi_{-2l})+2\cos(\phi_{-l}+\phi_0-\phi_{+l}-\phi_{-2l})\end{aligned}\tag{13}$$

from the phase equations.

Equations (12) and (13) provide general relations between the phases of the first five comb lines provided the dominant contributions to modes $\pm 2l$ have been effectively captured in Eqs. (9) and (10) and the amplitudes of the ± modes are approximately equal. If one takes the phases for modes 0 and $\pm l$ to be known, then Eqs. (12) and (13) become relations for the remaining unknown phases $\phi_{\pm 2l}$. For these equations to be simultaneously true across any general ϕ_0 and $\phi_{\pm l}$, one requires that

$$2\phi_{+l}-\phi_0-\phi_{+2l}=2\phi_{-l}-\phi_0-\phi_{-2l}.\tag{14}$$

This can be seen by equating the first (or second) terms of the left- and right-hand sides for either Eq. (12) or (13).

Equation (14) is a statement that the individual four-wave-mixing terms for the $+2l$ mode must separately balance their $-2l$ counterparts in the steady state, even if the individual $\phi_{\pm l}$ and $\phi_{\pm 2l}$ are asymmetric. The formulation of Eq. (14) is powerful as it can be applied to any higher-order mode. After going through analogous arguments, one finds a variety of four-wave-mixing contributions whose strengths vary greatly from one to the next. However, to satisfy the resulting equations of amplitude and phase for both the + and − modes, one requires the individual four-wave-mixing contributions between the ± modes to separately balance. This can be expressed generally as

$$\begin{aligned}&\phi_{al}+\phi_{bl}-\phi_{cl}-\phi_{(a+b-c)l}\\&\quad=\phi_{-al}+\phi_{-bl}-\phi_{-cl}-\phi_{-(a+b-c)l},\end{aligned}\tag{15}$$

where a, b, and c are integers. Note that Eq. (15) provides a general relationship between the phases of comb modes assuming a symmetric distribution of the mode amplitudes. However, within these constraints, the actual comb phase chosen will be the one that also maximizes the gain for each comb mode that forms. These results readily extend to all orders of the primary comb; however, care must be taken when applying Eq. (15) to the case of secondary bunched combs [19] whose characteristics are not currently fully understood.

We now return to our earlier discussion regarding the symmetry of the coupled-mode equations. As we have shown through Eqs. (14) and (15), even though the individual phases are asymmetric, the balance of the four-wave-mixing contributions maintains symmetry of the combined phases between the ± modes in Eq. (11). Since the coupled-mode equations cannot distinguish the individual + and − modes, the amplitudes of these modes must then also be equal in steady state. However, in practice, differences between the ± modes (e.g., the optical loss) prevent full symmetry between these modes.

III. NUMERICAL SIMULATIONS OF THE COMB PHASE

In this section we employ numerical simulation techniques for the purposes of understanding the complex phase behavior of the microresonator comb modes. Here we model the microresonator comb using the Lugiato-Lefever equation [15,17,26]. Compared to the modal expansion approach [22], the Lugiato-Lefever technique offers the advantage of lower computation times. The primary benefit of the modal expansion method is that it allows for greater control over each mode (in terms of specifying intermodal coupling, variations in loss, etc). However, this additional control is not necessary for our demonstrations here.

In terms of previous variable definitions, the Lugiato-Lefever equation can be expressed as [17]

$$\frac{\partial A}{\partial t}=-\frac{1}{2}\Delta\omega A-i\sigma A+\frac{1}{2}\Delta\omega F_0-ig_0|A|^2A-i\frac{\zeta_2}{2}\frac{\partial^2 A}{\partial\theta^2},\tag{16}$$

where A denotes the total field consisting of the superposition of all excited cavity modes. Here ζ_2 denotes the coefficient of second-order dispersion with mode number (or angular momentum eigenvalue) and θ denotes the azimuthal angle along the resonator's circumference. Figure 2(a) shows the normalized optical spectrum $|A(\omega)|^2$ of a microresonator comb simulated using Eq. (16). The simulations were carried out using the split-step Fourier method with the parameters $\Delta\omega = 5.0\times10^6$ rad/s, $\sigma = 0$ rad/s, $F_0 = 5.5\times10^4$, $g_0 = 2.4\times10^{-3}$ 1/s, and $\zeta_2 = 3.1\times10^4$ 1/s. Note that the value of $|F_0|^2$ in photons can be suitably converted into intracavity optical power once the cavity length and group velocity are specified. The buildup of the comb is initialized through noise injection, while the comb's steady-state operation corresponds to a mode spacing of 19 FSRs. The optical power decreases with increasing mode separation from ω_0, as is typical of comb states found through experimental measurement [11].

Figure 2(b) shows the corresponding phases of the individual comb lines. The phases are stationary as can be readily verified by computing the change in phase for each of the modes over time and showing this change to be approximately zero. Note that the group velocity motion has been translated out from Eq. (16) [17]. From Eq. (7) we expect that mode

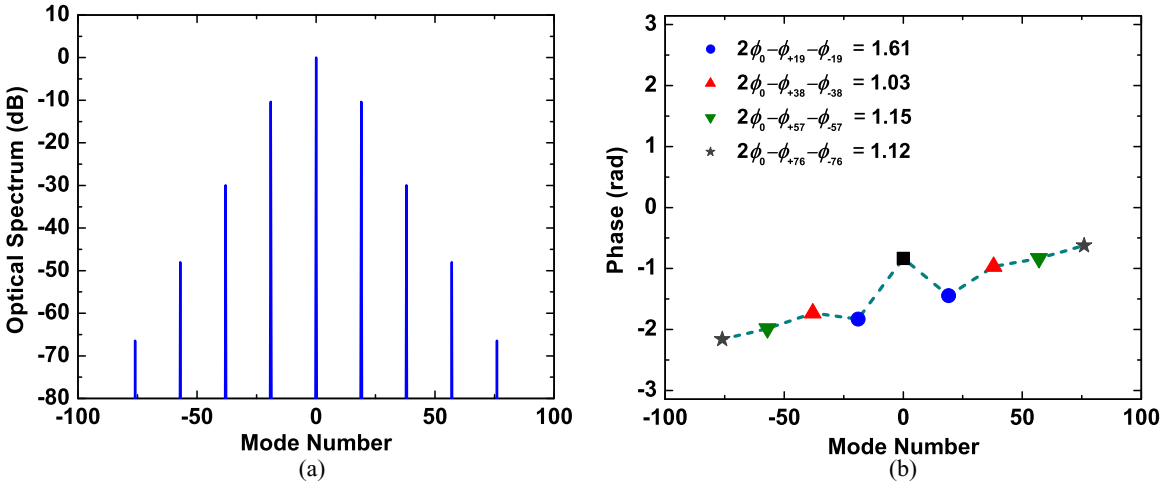

FIG. 2. (Color online) Simulated (a) optical spectrum and (b) phases of the modes for a microresonator comb with $\Delta\omega = 5.0 \times 10^6$ rad/s, $\sigma = 0$ rad/s, $F_0 = 5.5 \times 10^4$, $g_0 = 2.4 \times 10^{-3}$ 1/s, and $\zeta_2 = 3.1 \times 10^4$ 1/s.

0 and its first two adjacent comb lines jointly share a phase relationship that maximizes the gain of modes $\pm l$. However, we identified earlier that the presence of other interacting modes or the influence of a residual phase shift can spoil the phase relation between these modes. In Fig. 2(a) the higher-order comb lines are greatly attenuated (>20 dB) compared to the modes at $\pm l$ and thus are not expected to significantly alter the phase relationship of these modes. With one significant obstacle removed, Fig. 2(b) yields $2\phi_0 - \phi_l - \phi_{-l} = 1.61$ rad, which is close to the optimum value of $\pi/2$ rad. Note, however, that the phases of the higher-order modes do not satisfy Eq. (7) due to the contributions of the modes at $\pm l$, as can also be observed in Fig. 2(b). One can instead verify the phase sum on the left- and right-hand sides of Eq. (14). For the left-hand side, one finds a collective phase of -1.092 rad, while for the right-hand side, one find -1.092 rad. The agreement is excellent here and one can find similar levels of agreement ($<1 \times 10^{-5}$ rad phase difference) after testing *all* possible combinations according to Eq. (15).

Figure 3 shows one additional example of a microresonator comb simulated under a different set of operating conditions. The parameters used are $\Delta\omega = 5.0 \times 10^6$ rad/s, $\sigma = 2.1 \times 10^6$ rad/s, $F_0 = 8.8 \times 10^4$, $g_0 = 2.4 \times 10^{-3}$ 1/s, and $\zeta_2 = 1.5 \times 10^4$ 1/s. In this example, the laser is blue detuned and the anomalous dispersion is lower, so the modes reaching threshold must be located further away from the pump in order to cancel the cross-phase modulation. As a result, the mode spacing increases to 34 FSRs in this example. In the normalized optical spectrum of Fig. 3(a), the higher-order comb lines are again suppressed by >20 dB compared to the modes at $\pm l$.

Figure 3(b) shows the simulated phases corresponding to each of the individual comb lines. The variations in phase appear more chaotic than those found in Fig. 2(b). However, we can once again verify that $2\phi_0 - \phi_l - \phi_{-l} = 1.57$ rad here, nearly exactly reproducing the optimum value of $\pi/2$ rad. As in Fig. 2(b), the higher-order comb modes do not satisfy Eq. (7). Instead, we can determine the collective phases corresponding to the left- and right-hand sides of Eq. (14). The phase sum on the left-hand side evaluates to 5.214 rad, while the phase sum on the right-hand side yields 5.214 rad. Excellent agreement is again found here. After evaluating *all* possible combinations of modes [Eq. (15)], we determined the difference in phase to be $< 2.5 \times 10^{-5}$ rad from the expected phase relationship.

IV. EXPERIMENTAL MEASUREMENTS OF THE COMB PHASE

In this section we provide independent experimental verification of the microcomb phase [Eq. (7)] by directly measuring the phase relationship among the central three comb lines. The phases of the higher-order comb lines become more difficult to analyze in our setup configuration due to their significantly lower optical power. The setup for the phase measurement is illustrated in Fig. 4. A tunable laser source set to 1553 nm is first sent through a circulator, which directs ~60 mW of optical power through a tapered fiber. The tapered fiber allows for efficient coupling of the optical power into a fused silica microrod resonator (diameter equal to 2.6 mm, FSR of 25.6 GHz, and loaded $Q = 1.85 \times 10^8$). Through the Kerr nonlinearity of the resonator, a comb is generated that can be analyzed in transmission on an optical spectrum analyzer (OSA). Because the comb output of the resonator mixes with the fraction of the laser pump that passes by the resonator, the phase of the fundamental comb line cannot be accurately determined.

We instead analyze the comb lines in reflection, amplifying the reflected signal and sending the resulting signal through a liquid-crystal programmable waveshaper. The waveshaper allows for both amplitude and phase control of each of the individual comb lines and thus is the essential component enabling the measurement of phase. The output of the waveshaper is amplified a second time and finally is sent into a second-order intensity autocorrelator and oscilloscope for measurement of the time-domain pulse. Note that care must be taken when analyzing the phases of the backreflected comb. If the backreflection is due to multiple randomly distributed scattering sites rather than to one dominant source of reflection, then the amplitude and phase of the comb lines will become imbalanced due to the interference of the backscattered fields.

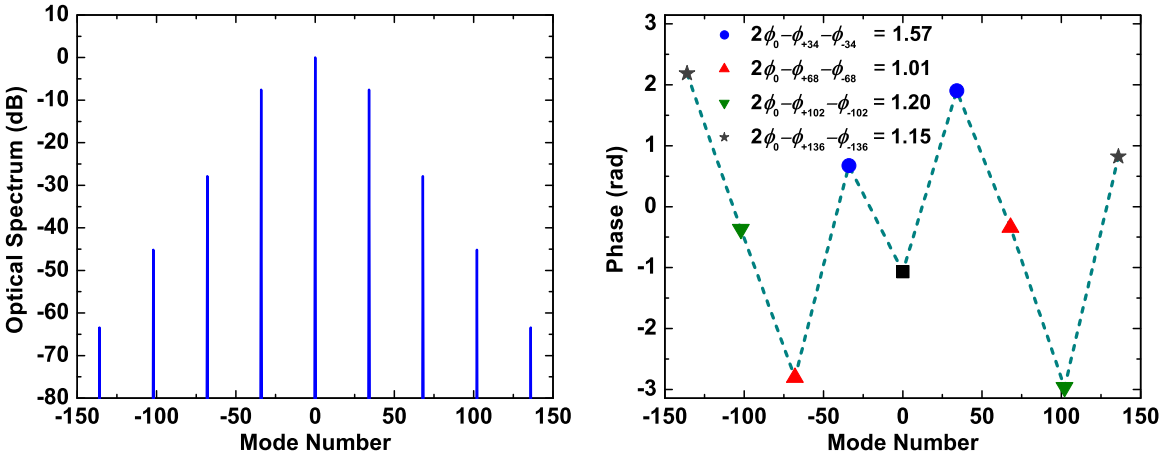

FIG. 3. (Color online) Simulated (a) optical spectrum and (b) phases of the modes for a microresonator comb with $\Delta\omega = 5.0 \times 10^6$ rad/s, $\sigma = 2.1 \times 10^6$ rad/s, $F_0 = 8.8 \times 10^4$, $g_0 = 2.4 \times 10^{-3}$ 1/s, and $\zeta_2 = 1.5 \times 10^4$ 1/s.

However, in our measurements, we observed no significant asymmetry of the three central comb lines.

By adjusting the phase of each individual comb line, one can determine the optimum arrangement of phase so that the peak of the autocorrelation trace is maximized [11,18,27]. It can be shown that the maximum in the autocorrelation occurs when the phases of the individual comb lines are aligned. However, we note that this optimum configuration of phase is *not* unique. For example, the translation of each comb line by a constant but arbitrary phase shift yields the same autocorrelation. Furthermore, a linear slope in phase corresponds to an additional group delay and thus also does not distort the pulse waveform. Fortunately, the operation $2\phi_0 - \phi_l - \phi_{-l}$ is insensitive to both of these cases.

Figure 5(a) shows the spectrum of a microresonator comb in transmission centered on the pump wavelength at 1553 nm. The comb was specifically operated such that the higher-order comb modes are significantly lower in power (>12 dB) compared to modes $0, \pm l$. This minimizes the impact of these higher-order modes on the phase measurement.

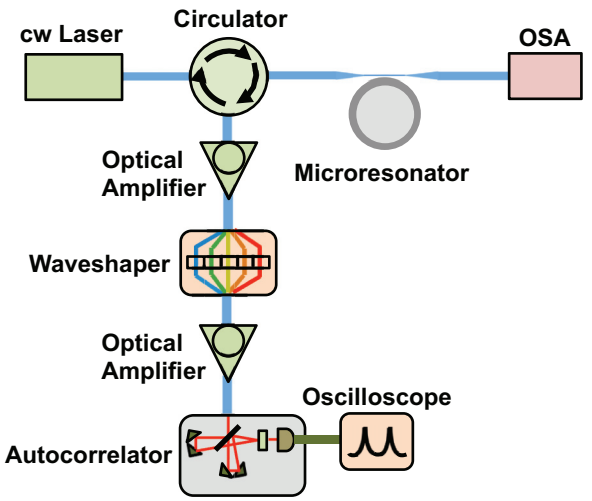

FIG. 4. (Color online) Illustration of the experimental setup used for measuring the phases of the individual comb lines.

Figure 5(b) shows measurements of $2\phi_0 - \phi_l - \phi_{-l}$ (in reflection) for the microresonator comb state shown in Fig. 5(a). We disconnect all equipment from the taper coupler in the forward direction, leaving only an unterminated angle-polished interface. This minimizes the effect of spurious backreflections. The dispersion of the measurement setup was separately measured and accounted for by application of a test pulse through the entirety of our measurement system. By measuring the pulse autocorrelation before and after the setup, one can then determine the necessary dispersion map applied by the waveshaper to cancel the dispersion of the setup. Our measurements consist of nine trials varying both the initial starting amplitudes and phases of modes $0, \pm l$. The phase is then sequentially scanned for each of the three modes from 0 to $(2\pi \times 13)/14$ in 14 steps. The optimum applied phase that maximizes the peak of the autocorrelation trace can be inverted to determine the actual phase of each mode. Because the optimum phase is not unique (see previous discussion), the phase for each mode changes from one trial to the next. However, the operation $2\phi_0 - \phi_l - \phi_{-l}$ consistently yields near $\pi/2$ rad as predicted by Eq. (7). Note that the average phase of $2\phi_0 - \phi_l - \phi_{-l}$ over all nine measurements is 1.69 rad with a standard deviation of the mean of 0.13 rad. The theoretical phase of $\pi/2$ rad is within these bounds. Coupled with the limitations from a relatively large scan step size of 0.45 rad, which yields a maximum phase error of 0.225 rad [18], we see that the theory, simulations, and experimental measurement are all in good agreement. Note in addition that if σ_l does not exactly compensate $-2g_0|B_0|^2$ as in Eq. (8), it also becomes possible for $2\phi_0 - \phi_l - \phi_{-l}$ to deviate from $\pi/2$ rad (see Sec. II).

V. UNIFORMITY OF THE COMB FREE SPECTRAL RANGE

In the previous sections we showed that the operation of the microresonator comb does not necessitate the comb lines to have equal phase. Here we utilize this understanding of phase to investigate one additional property related to the coherence of the microresonator comb, namely, the uniformity of the

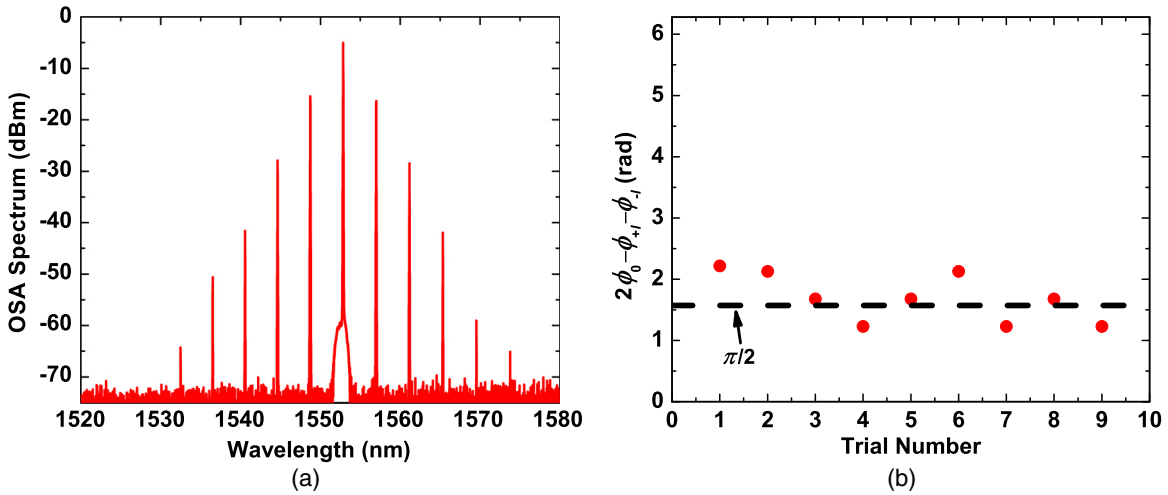

FIG. 5. (Color online) Experimentally measured (a) optical spectrum in transmission and (b) phase difference of modes $0, \pm l$ in reflection for a microresonator comb.

comb FSR (also known as mode offsets). It is well known when the secondary bunched comb lines form in between the modes of the primary comb, they can be offset from being a subharmonic of the original FSR [19,20] (see Fig. 6). Considerable analysis on the formation of secondary comb lines has been previously performed in Ref. [19]. Here we use the diagram of Fig. 1 to further supplement the current state of knowledge regarding the origin of these shifts. In particular, unlike previous treatments of the secondary comb, our analysis introduces the possibility of a variable frequency shift during the formation of the secondary comb lines.

To simplify the more general Eq. (1) to that of Eq. (2), we introduced a change of variables $B_0 = A_0 e^{-i\sigma t}$ and $B_{\pm l} = A_{\pm l} e^{-i(\sigma+\varpi_l/2)t}$ such that the comb lines were translated into equidistance. Here the frequency shifts were identical for the lines at $\pm l$; however, in theory these shifts can be asymmetric. That is, ignoring detuning for simplicity, *any* combined shift of both comb lines that sums to ϖ_l (e.g., $\varpi_l/2+\delta$ and $\varpi_l/2-\delta$ with frequency offset δ) not only would translate these lines to equidistance and satisfy energy conservation, but also would remove the time dependence of Eq. (1). Yet we have chosen the symmetric arrangement in Eq. (2) with each comb line translated by a single dispersion step. The essential point is that any asymmetric configuration of translations would yield asymmetry in the phase shifts accumulated for modes $\pm l$ [Eq. (2), second term on the right-hand side of the second equation]. This asymmetry prevents both modes from simultaneously compensating the cross-phase modulation of the pump wave [Eq. (4)].

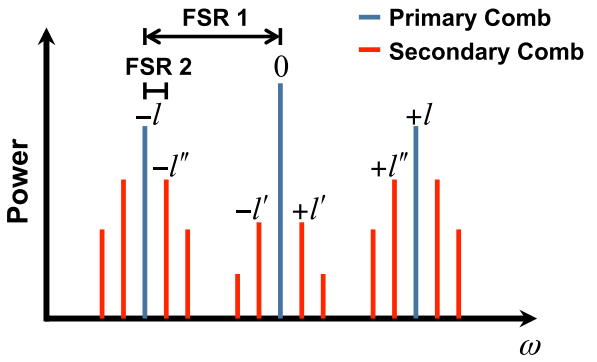

FIG. 6. (Color online) Illustration of the FSR shift between a primary comb and a secondary comb.

Such a situation is unstable, as can be seen from Eq. (8) with K replaced by $K_{\pm l} = -(\sigma_l \pm \delta) - 2g_0|B_0|^2$. Next, defining $B_{\pm l} = |B_{\pm l}|e^{i\phi_{\pm l}}$ and $B_0 = |B_0|e^{i\phi_0}$, one can reduce Eq. (8) into the following set of evolution equations for amplitude and phase:

$$\frac{d|B_{\pm l}|}{dt} = -\frac{1}{2}\Delta\omega|B_{\pm l}| + g_0|B_0|^2\,|B_{\mp l}|\sin(2\phi_0-\phi_l-\phi_{-l}),$$
$$\frac{d\phi_{\pm l}}{dt} = -g_0\frac{|B_0|^2\,|B_{\mp l}|}{|B_{\pm l}|}\cos(2\phi_0-\phi_l-\phi_{-l}) + K_{\pm l}. \quad (17)$$

From the phase equation, it is clear that no steady-state solution is possible if the sign of $K_{\pm l}$ flips between modes $\pm l$ as would be the case if $\delta \neq 0$ and the detuning and dispersion exactly balanced the cross-phase modulation for modes $\pm l$. This results because only one source of gain is available to simultaneously compensate for two distinct phase rotations. If the two modes are chosen such that the values of $K_{\pm l}$ are the same sign, then one could possibly vary the individual amplitudes of $|B_{\pm l}|$ such that with the appropriate combination of phases, $d\phi_{\pm l}/dt$ becomes zero for modes $\pm l$. However, this steady-state solution would then prevent both modes from simultaneously reaching $d|B_{\pm l}|/dt = 0$. Therefore, the symmetry of the system forces $\delta = 0$ for the first two $\pm l$ modes that form.

One can readily extend Eq. (17) to the higher-order comb lines generated beyond modes $\pm l$. However, such an analysis was already performed in Eqs. (9) and (10) with the resulting frequency shift of the modes constrained by the previous comb lines. This occurs because with all the other comb lines of the cascaded four-wave-mixing process already set, the only frequency translation that maintains energy conservation and removes the time dependence in the coupled-mode equations is the one where the FSR of the primary comb is maintained. In other words, the original comb lines act as a mold for where the subsequent primary comb lines must fall.

We now apply the same procedure to the generation of the secondary bunched comb lines. We do this for mode $+l''$ (see Fig. 6), identifying its time evolution to follow the form of

$$\begin{aligned}\frac{dA_{\pm l''}}{dt} &= -\frac{1}{2}\Delta\omega A_{\pm l''} - 2ig_0|A_0|^2 A_{\pm l''} \\ &\quad - ig_0 A_0^2 A^*_{\mp l''} e^{i(2\omega_0-\omega_{-l''}-\omega_{l''})t} \\ &\quad - 2ig_0 A_0 A_{\pm l} A^*_{\pm l'} e^{i(\omega_0+\omega_{\pm l}-\omega_{\pm l'}-\omega_{\pm l''})t}, \end{aligned} \quad (18)$$

where $A_{\pm l'}, A_{\pm l''}$ and $\omega_{\pm l'}, \omega_{\pm l''}$ denote the complex amplitudes and angular frequencies of modes $\pm l', \pm l''$. Equation (18) assumes for simplicity that the pump wave dominates the cross-phase modulation contribution and also includes only the strongest interactions between modes. Note that Eq. (18) is comparable to Eq. (1) for modes $\pm l$, but with an additional term denoting the four-wave-mixing contribution from higher-order modes.

We now introduce the mapping $B_0 = A_0 e^{-i\sigma t}$, $B_{\pm l} = A_{\pm l} e^{-i(\sigma+\varpi_l/2)t}$, $B_{\pm l'} = A_{\pm l'} e^{-i(\sigma+\varpi_{l'}/2\mp\delta)t}$, and $B_{\pm l''} = A_{\pm l''} e^{-i(\sigma+\varpi_{l''}/2\pm\delta)t}$ into Eq. (18) with δ serving the role of a variation in the frequency translation. Here $\varpi_{l'} = 2\omega_0 - \omega_{l'} - \omega_{-l'}$ and $\varpi_{l''} = 2\omega_0 - \omega_{l''} - \omega_{-l''}$. Thus δ appears as an adjustable frequency shift on the modes $\pm l', \pm l''$ similar to that shown in Fig. 1. With this mapping scheme and assuming negligible influence from higher-order dispersion processes (beyond second order), Eq. (18) transforms into

$$\begin{aligned}\frac{dB_{\pm l''}}{dt} &= -i\left(\sigma + \frac{1}{2}\varpi_{l''} \pm \delta\right) B_{\pm l''} - \frac{1}{2}\Delta\omega B_{\pm l''} \\ &\quad - 2ig_0|B_0|^2 B_{\pm l''} - ig_0 B_0^2 B^*_{\mp l''} - 2ig_0 B_0 B_{\pm l} B^*_{\pm l'}. \end{aligned} \quad (19)$$

Unlike the higher-order modes of the primary comb, the modes of the secondary comb admit the possibility of a frequency shift as long as the sign of δ is carefully chosen in the mapping so that comb lines $\pm l', \pm l''$ shift together in synchrony. Our previous analysis of modes $\pm l$ also showed that a frequency shift δ was possible in the coupled-mode equations. However, we later found this frequency shift to be unstable in the steady state (Eq. 17).

Continuing with our analysis, we define $B_0 = |B_0|e^{i\phi_0}$, $B_{\pm l} = |B_{\pm l}|e^{i\phi_{\pm l}}$, $B_{\pm l'} = |B_{\pm l'}|e^{i\phi_{\pm l'}}$, and $B_{\pm l''} = |B_{\pm l''}|e^{i\phi_{\pm l''}}$, thereby separating Eq. (19) into its evolution equations for amplitude and phase

$$\begin{aligned}\frac{d|B_{\pm l''}|}{dt} &= -\frac{1}{2}\Delta\omega|B_{\pm l''}| + g_0|B_0|^2|B_{\mp l''}| \\ &\quad \times \sin(2\phi_0 - \phi_{-l''} - \phi_{l''}) \\ &\quad + 2g_0|B_0||B_{\pm l}||B_{\pm l'}|\sin(\phi_0 + \phi_{\pm l} - \phi_{\pm l'} - \phi_{\pm l''}), \\ \frac{d\phi_{\pm l''}}{dt} &= -\left(\sigma + \frac{1}{2}\varpi_{l''} \pm \delta\right) - 2g_0|B_0|^2 \\ &\quad - g_0\frac{|B_0|^2|B_{\mp l''}|}{|B_{\pm l''}|}\cos(2\phi_0 - \phi_{-l''} - \phi_{l''}) \\ &\quad - 2g_0\frac{|B_0||B_{\pm l}||B_{\pm l'}|}{|B_{\pm l''}|}\cos(\phi_0 + \phi_{\pm l} - \phi_{\pm l'} - \phi_{\pm l''}). \end{aligned} \quad (20)$$

There are two possible scenarios worth consideration in Eq. (20). The first scenario is that the phases of the l'' mode $(\phi_0 + \phi_l - \phi_{l'} - \phi_{l''})$ exactly balance the phases of the $-l''$ mode $(\phi_0 + \phi_{-l} - \phi_{-l'} - \phi_{-l''})$, as would normally be the case for the primary comb lines. If the phases of the $\pm l'$ evolution equations (not shown) are also balanced, the symmetry in the amplitude equations then forces equality in the amplitudes of the $\pm l''$ modes and also of the $\pm l'$ modes. With both the phase and amplitude balanced, the steady state for the evolution of phase in Eq. (20) requires that $\delta = 0$. Thus, we see that no shift in frequency is present for this scenario and the secondary modes that form are at a subharmonic of the primary comb spacing.

The second case we consider here is that the phases are unbalanced between the $\pm l''$ modes. Unlike our analysis of the primary comb earlier [Eq. (11)], a phase imbalance appears possible here as the frequency shift δ can absorb the differences that arise in the four-wave-mixing contributions. However, we note that the amplitude evolution equations predict at least some degree of amplitude asymmetry for this case. The optimum configuration is the one where the gain is maximized for modes $\pm l'$ and $\pm l''$. This will in general depend on the operating conditions (pump power and detuning) and system material parameters (dispersion and strength of optical nonlinearity). The mode translation picture of Fig. 1 is therefore expected to serve as a useful tool for analyzing the spacing and equidistance of the lines generated from a microresonator comb.

VI. CONCLUSION

In this work we discussed the fundamental operation of the microresonator comb, analyzing in particular the phase and coherence of the comb spectrum. Our main goal was to show that even with a coherent nonlinear process, the comb modes in many cases do not stabilize around identical phase. Through symmetry arguments, one finds instead specific phase relationships that the fields of the primary comb must satisfy. Under ordinary operating conditions, these phase relationships lead to a symmetrical spectral arrangement in amplitude but a disordered arrangement in phase. We used a combination of numerical simulation and experimental measurement to support our theoretical analysis. As a secondary point of study, we applied our discussion of comb phase to the investigation of the multiple FSRs generated within a secondary comb spectrum. Our results therefore reveal the complexities in the operation of a microresonator comb that require further understanding before mode-locked comb states producing short pulses can be consistently generated.

ACKNOWLEDGMENTS

This work was funded by NIST, DARPA QuASAR, and AFOSR. W.L. acknowledges support from the NRC/NAS. This work is a contribution of the US Government and is not subject to copyright in the US.

[1] J. Ye and S. T. Cundiff, *Femtosecond Optical Frequency Comb Technology: Principle, Operation, and Application* (Springer, Berlin, 2005).
[2] S. T. Cundiff and J. Ye, Rev. Mod. Phys. **75**, 325 (2003).
[3] J. Ye, H. Schnatz, and L. Hollberg, IEEE J. Quantum Electron. **9**, 1041 (2003).
[4] T. Udem, R. Holzwarth, and T. W. Hänsch, Nature (London) **416**, 233 (2002).
[5] T. Steinmetz, T. Wilken, C. Araujo-Hauck, R. Holzwarth, T. W. Hansch, L. Pasquini, A. Manescau, S. D'Odorico, M. T. Murphy, T. Kentischer, W. Schmidt, and T. Udem, Science **321**, 1335 (2008).
[6] T. M. Fortier, M. S. Kirchner, F. Quinlan, J. Taylor, J. C. Bergquist, T. Rosenband, N. Lemke, A. Ludlow, Y. Jiang, C. W. Oates, and S. A. Diddams, Nat. Photon. **5**, 425 (2011).
[7] P. Del'Haye, A. Schliesser, O. Arcizet, T. Wilken, R. Holzwarth, and T. J. Kippenberg, Nature (London) **450**, 1214 (2007).
[8] T. J. Kippenberg, R. Holzwarth, and S. A. Diddams, Science **332**, 555 (2011).
[9] I. S. Grudinin, N. Yu, and L. Maleki, Opt. Lett. **34**, 878 (2009).
[10] M. A. Foster, J. S. Levy, O. Kuzucu, K. Saha, M. Lipson, and A. L. Gaeta, Opt. Express **19**, 14233 (2011).
[11] S. B. Papp and S. A. Diddams, Phys. Rev. A **84**, 053833 (2011).
[12] T. Herr, V. Brasch, J. D. Jost, C. Y. Wang, N. M. Kondratiev, M. L. Gorodetsky, and T. J. Kippenberg, Nat. Photon. **8**, 145 (2014).
[13] K. Saha, Y. Okawachi, B. Shim, J. S. Levy, R. Salem, A. R. Johnson, M. A. Foster, M. R. E. Lamont, M. Lipson, and A. L. Gaeta, Opt. Express **21**, 1335 (2013).
[14] A. B. Matsko, A. A. Savchenkov, W. Liang, V. S. Ilchenko, D. Siedel, and L. Maleki, Opt. Lett. **36**, 2845 (2011).
[15] S. Coen, H. G. Randle, T. Sylvestre, and M. Erkintalo, Opt. Lett. **38**, 37 (2013).
[16] M. R. E. Lamont, Y. Okawachi, and A. L. Gaeta, Opt. Lett. **38**, 3478 (2013).
[17] Y. K. Chembo and C. R. Menyuk, Phys. Rev. A **87**, 053852 (2013).
[18] P. Del'Haye, S. B. Papp, and S. A. Diddams, Phys. Rev. Lett. **112**, 043905 (2014).
[19] T. Herr, K. Hartinger, J. Riemensberger, C. Wang, E. Gavartin, R. Holzwarth, M. L. Gorodetsky, and T. J. Kippenberg, Nat. Photon. **6**, 480 (2012).
[20] S. B. Papp, P. Del'Haye, and S. A. Diddams, Opt. Express **21**, 17615 (2013).
[21] R. W. Boyd, *Nonlinear Optics* (Elsevier, Amsterdam, 2008).
[22] Y. K. Chembo and N. Yu, Phys. Rev. A **82**, 033801 (2010).
[23] Y. K. Chembo, D. V. Strekalov, and N. Yu, Phys. Rev. Lett. **104**, 103902 (2010).
[24] Y. K. Chembo and N. Yu, Opt. Lett. **35**, 2696 (2010).
[25] J. Hansryd, P. A. Andrekson, M. Westlund, J. Li, and P. O. Hedekvist, IEEE J. Sel. Top. Quantum Electron. **8**, 506 (2002).
[26] L. A. Lugiato and R. Lefever, Phys. Rev. Lett. **58**, 2209 (1987).
[27] F. Ferdous, H. X. Miao, D. E. Leaird, K. Srinivasan, J. Wang, L. Chen, L. T. Varghese, and A. M. Weiner, Nat. Photon. **5**, 770 (2011).